Investigation of hazelnut shells driven hard carbons as anode for sodium-ion batteries produced by hydrothermal carbonization method

Elif CANBAZ, **Meral AYDIN**, **Rezan DEMİR-ÇAKAN***
Department of Chemical Engineering, Gebze Technical University, Kocaeli, Turkey

Abstract: To be used as Na-ion battery anodes, hard carbon electrodes are synthesized from biomass, explicitly hazelnut shell (HS): via hydrothermal carbonization (HTC) followed by further pyrolysis at different temperatures (500, 750, 1000 °C). Then, the resulting hazelnut shell-based hard carbons are investigated using various methods including Fourier-transform infrared spectroscopy, scanning electron microscope, X-ray diffraction, galvanostatic charge/discharge, and electrochemical impedance spectroscopy. The effects of binders (PVdF, Na-alginate, CMC, and PAA) on electrochemical performance are determined. The obtained composite electrodes with different binders are tested in sodium half-cell configurations. A strong correlation is recognized between carbonization temperature and electrochemical performances and structural characteristics. The better cycling performance is accomplished with the electrode carbonized at 1000 °C with Na-alginate binder. After 100 cycles, specific capacity of 232 mAh × g^{-1} at 0.1C current density is achieved. This work represents an economical and feasible process to convert hazelnut shells into hard carbon.

Key words: Hard carbon, hydrothermal carbonization, sodium ion batteries, bio-waste

1. Introduction

As a result of the growing industries and the irreversible depletion of fossil fuels, energy demand is tremendously increasing. Thus, the development of alternative energy sources, energy storage strategies and conversion devices such as fuel cell, capacitors and batteries are necessary. Among them, lithium-ion battery (LIB) technologies are widely used for mobile electronic devices and electric vehicles because of its high energy and power density and long cycle life [1-3]. The increasing demand of the battery market and depletion of lithium resources require alternative battery chemistries. Sodium-ion batteries (SIBs) have received much attention as one of the most promising candidates for electrical energy storage because of the abundance, wide availability of sodium resources, and chemical similarities of sodium to lithium [4,5].

However, the major challenge in commercializing sodium ion battery technology depends on finding suitable electrode materials, especially anode materials. Graphite is the most widely used anode material in LIBs due to its abundant resource, electronic conductivity, and cycling stability. However, ionic size of sodium ions is larger than lithium (1.02 Å of Na$^+$ vs 0.76 Å of Li$^+$) and it is not suitable for layer distance of graphite with conventional carbonate-based electrolytes [6,7]. Direct use of sodium metal as an anode causes some problems such as poor performance, easy short circuit, high chemical reactivity, and dendrite formation [8]. Up to now, anode materials with different ion storage mechanisms (based on the insertion, conversion and alloying reactions) have been researched by using carbon materials [9-11], transition metal oxides [12,13], alloys [14-16], or organic compounds [17-19]. Most of the anode materials (i.e. Sn, Sb or their oxides, sulfides, or alloys) used in the field of Na-ion batteries suffer from the large volume expansion during sodium ion insertion. On the other hand, organic compounds have insufficient cycling stability and low conductivity [6, 20]. Hard carbon is the most promising carbon anode material because of its large interlayer distance of the disordered carbon structure, and they can be prepared via simple conversion process of waste biomass [21,22].

In this study, we derived hard carbon material from hazelnut shell (HS) with two step carbonization processes: hydrothermal carbonization (HTC) and further carbonization at different temperatures. HS is a great energy potential of Turkey since it holds 75% of planted areas in the world [23]. The shells of hazelnut are important agricultural residues and represents approximately 50 wt.% of total hazelnuts. The structure of HS consists of cellulose and hemicellulose indicating

* Correspondence: demir-cakan@gtu.edu.tr

that HS is a suitable carbon source to produce hard carbon [24]. Herein, we propose an efficient, low-cost, and simple method to synthesize hard carbon by using bio-waste. Firstly, HTC process was applied under mild reaction conditions and then further carbonization was applied at three different temperatures (500, 750, and 1000 °C). Finally, the resulting HS-derived hard carbon electrodes were performed as anode materials for sodium-ion battery.

2. Experimental

2.1. Materials

Hazelnut shell was collected from Trabzon, Turkey. Propylene carbonate (PC) (Sigma Aldrich): ethylene carbonate (EC) (Sigma Aldrich): sodium perchlorate ($NaClO_4$) (Alfa Aesar): were used for electrolyte preparation. Polyvinylidene fluoride (PVdF) (Alfa Aesar) and carboxy methyl cellulose (CMC) (Doga Nanobiotech): Na-alginate (Alfa Aesar): polyacrilic acid (PAA) (Sigma Aldrich) were used as binders and 1-methyl-2-pyrrolidone (NMP) (Alfa Aesar) was used as a dissolving solvent of PVdF.

2.2. Synthesis of HS-derived hard carbon

HS-derived hard carbon anode material was synthesized with two different routes with/without HTC. For HTC, the collected shells were pulverized to obtain HS powder. Then, 0.5 g of HS powder, 18 mL distilled water and two drops of sulfuric acid (as a catalyst) were mixed. The mixture was transferred into Teflon-lined stainless-steel autoclave and synthesis was carried out under mild temperature (200 °C during 48 h rest time) in an oven. After HTC process, the sample was cooled down to room temperature and washed with pure water and ethanol, respectively. Resulting hydrochar sample was dried in an oven at 80 °C for 12 h.

Moreover, further carbonization process was performed to the hydrochar at various temperatures (500, 750, and 1000 °C) with heating rate of 2 °C min⁻¹ under N_2 atmosphere for 6 h in tubular furnace. Synthesized carbon materials were quoted as HS-HTC, HS-HTC@500, HS-HTC@750, HS-HTC@1000. For the sake of comparison, carbon materials without HTC process were also prepared. Direct carbonization of the HS powder was named as HS@500, HS@750, and HS@1000. The overall procedure is illustrated in Figure 1.

2.3. Physical characterizations

The thermal history and decomposition temperature of raw HS was characterized by thermogravimetric analysis (TGA) measurements (Perkin Elmer, 4000) performed at a heating rate of 10 °C min⁻¹ between room temperature and 900 °C in an Argon atmosphere. The level of structural order of bare HS, hydrochar, and hard carbon were characterized by X-ray diffraction (XRD Bruker D8 Advance diffractometer (θ-2θ mode, Cu Kα radiation, λ = 1.5406): measurement was carried out in the range of 10–90 degrees and at a scanning speed of 2° min⁻¹. The morphology of materials was investigated by scanning electron microscopy (SEM) (Philips XL30). Functional groups on bare HS and the resulting carbon materials were determined via Fourier-transform infrared spectroscopy (FTIR) spectroscopy (Perkin Elmer Spectrum 100).

2.4. Electrochemical measurements

The electrochemical performance of HS-derived electrodes was investigated by coin type cells assembled in an Argon filled glovebox. The working electrode was prepared by mixing active material with different binders (polyvinylidene fluoride (PVdF): carboxy methyl cellulose (CMC): Na-alginate, polyacrylic acid (PAA)), and super-P carbon at a weight ratio of 8:1:1. N-methyl-2-pyrrolidone (NMP, for PVdF binder) and distilled water (for CMC, Na-alginate, PAA binders) were used as dispersion mediums. Then, the slurry was laminated on copper foil and dried in a vacuum oven for 12 h. Na foil was used as both counter and reference electrodes. 1 M $NaClO_4$ ethylene carbonate/propylene carbonate was used as electrolyte. Galvanostatic charge/discharge measurements were carried out on the battery tester (Neware) at 0.005–2 V (vs Na/Na⁺) and 0.1C current density (1 C = 372 mAh × g⁻¹). Electrochemical Impedance Spectroscopy (EIS) measurements were performed between the frequency range of 1 MHz and 10 kHz with voltage amplitude of 5 mV (VMP3 Bio-Logic). Cyclic voltammetry (CV) tests (Biologic VMP-3 electrochemical Workstation) were carried out in the voltage range of 0.005–2 V at various scan rates (0.2, 0.1, 0.05, 0.01 mV × s⁻¹) to determine capacitive and diffusion controlled contribution.

3. Results and discussion

3.1. Material characterizations

There is a wide variety of biomass on earth and all of them have unique microstructure. These structural diversities directly affect the nature of the produced hard carbons. Ultimately, sodium ion diffusion and storage capacity depend on the structure of electrode materials [25]. Based on the analysis (wt.% of dry and ash free shell) hazelnut shell (HS) contains 50.8% of carbon, 42.6% of oxygen, 1.4% of nitrogen, and 5.2% hydrogen [26]. The amount of carbon contained in HS indicates that HS is a convenient raw material for the preparation of hard carbon materials. To investigate the thermal

history and decomposition of raw HS, TGA was performed with temperature range from room temperature to 900 °C, as shown in Figure 2a. The TGA curve shows an initial mass loss of nearly 8% at 90 °C corresponding to moisture release. In addition, largest mass loss (50%) was observed at around 375 °C that could be attributed to the decomposition of cellulose/hemicellulose. On the other hand, lignin was decomposed in the temperature range of 175–600 °C and the significant mass loss was not observed when the temperature is higher than 600 °C. After all, the thermal decomposition process yield is 35.57%. To sum up, lignocellulosic materials are known to be decomposed above 200 °C [27,28] as we have also observed with the TGA measurement. Furthermore, the electrochemical performances of the resulting electrodes differ with the final carbonization temperatures [29,30]. Thus, in this research paper, we have carbonized the samples in three different temperatures and reported their electrochemical performances. Structural characterization and surface morphology of the materials were investigated with SEM, XRD, and FTIR measurements. XRD patterns of HS-derived hard carbon materials and hydrochar are shown in Figure 2b. HS-HTC@1000 has two broad peaks around 23º and 43º corresponding to (0 0 2) and (1 0 1) graphitic planes, respectively [31,32]. XRD patterns prove that the biomass-derived hard carbon is between amorphous and graphite (turbostratic) structures where graphene layers randomly sorted on each other. Intensity of the peaks increases with rising the carbonization temperature. Functional groups of bare HS, HS-HTC, and HS-HTC@1000 were examined by FTIR analysis (Figure 2c). The large absorption band seen at 3500–3000 cm^{-1} for HS and HS-HTC samples shows the presence of hydroxyl groups in the structure. HTC process has a step of aromatization, 750 cm^{-1} band can be attributed to the aromatic rings of the structure [33]. For bare HS and HS-HTC, the peak observed around 1690 cm^{-1} can be assigned to the C=O vibrations and these peaks were disappeared after carbonization process. Functional groups on surface can easily react with sodium ions and cause irreversible capacity losses [21].

Depending on the SEM images of the bare HS, characteristic lignocellulosic structure, fibrous and sheet-like structures were observed (Figure 3). After the HTC process was applied, these fibrous structures began to be replaced by spherical microparticles since carbon formation through the HTC process relies on the emulsion polymerization like mechanism
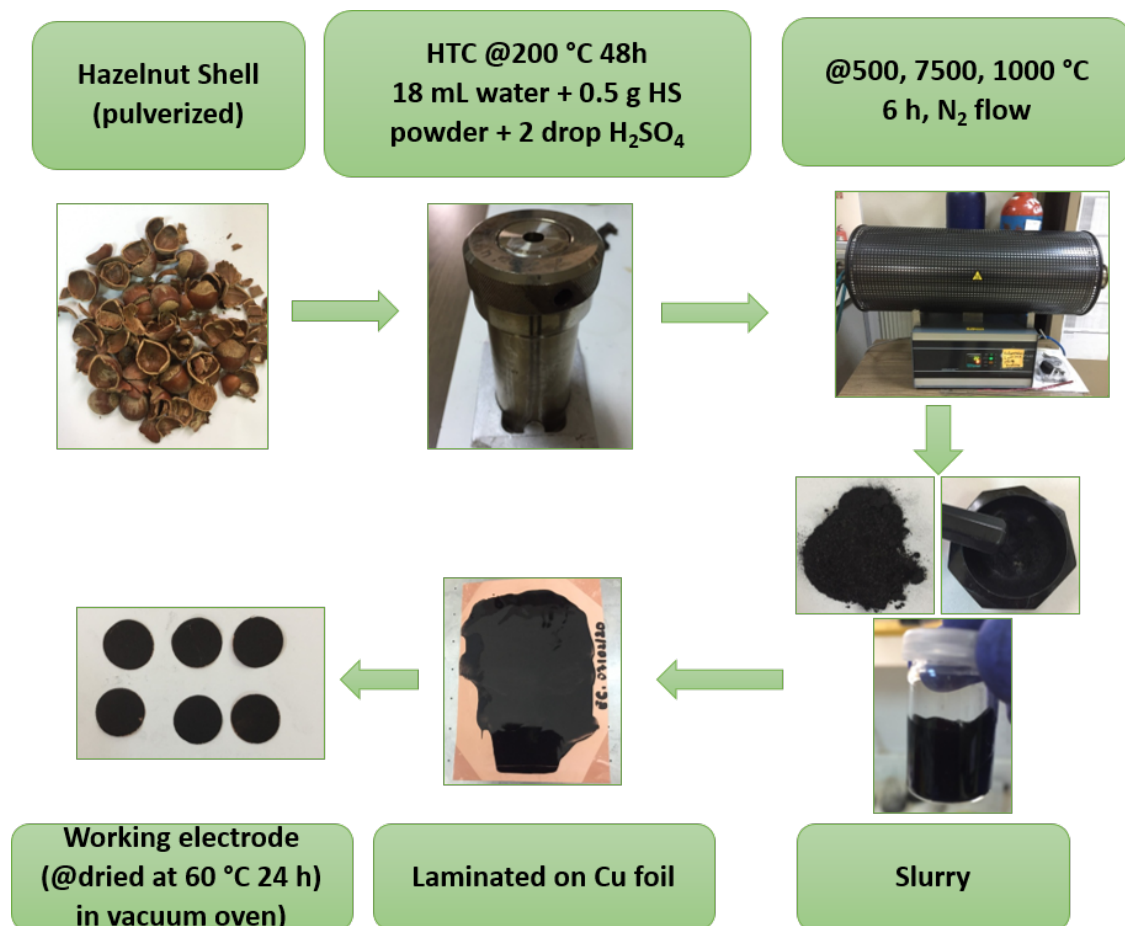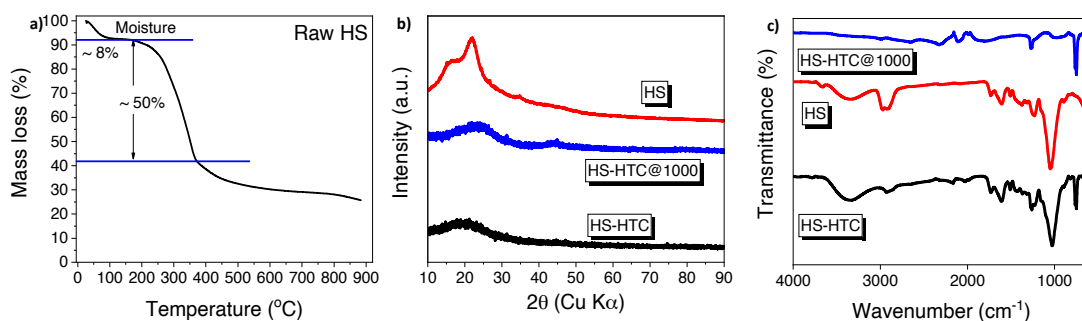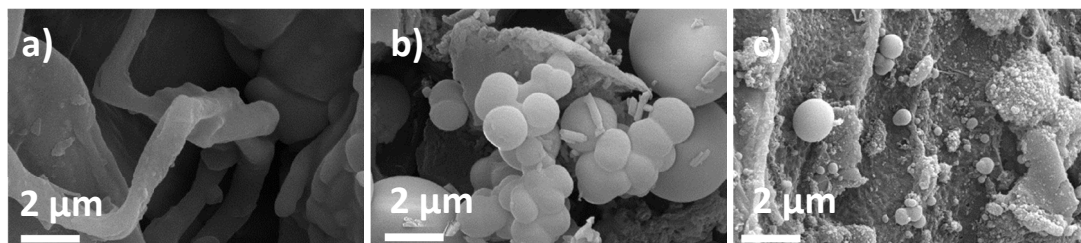

Figure 1. Schematic representation of the HS-derived hard carbon electrode.

Figure 2. a) TGA data of raw HS at a heating rate of 10 °C min^{-1} under an Ar atmosphere b) XRD patterns of HS-HTC and HS-HTC@1000, c) FTIR spectra of bare HS, HS-HTC, and HS-HTC@1000.

Figure 3. SEM images of a) bare HS, b) HS-HTC, c) HS-HTC@1000.

[21]. From the observations of SEM images, spherical microparticles transform into porous carbon structures by further increasing carbonization temperature to 1000 °C. Well-developed porous structure not only decreases the diffusion path of sodium ions but also enables electrolyte penetration into electrode.

Hydrochar contains functional group on its surface and has an amorphous structure. HTC process yields a low-grade of carbonization accompanied with the low degree of electrical conductivity. At this stage, cellulosic network does not completely degrade; thus, higher temperatures are needed [34,35]. Therefore, further carbonization process was applied to improve level of structural order.

3.2. Electrochemical characterizations

The electrochemical characterizations of hard carbon electrodes were tested as anode materials for sodium ion battery by using half-cell configurations. Figure 4 represents the impact of different carbonization temperature on electrochemical performance of HS-derived hard carbon anode. Electrochemical performances were tested with galvanostatic charge/discharge cycling at 0.1C (1C = 372 mAh $\times$ g^{-1}) current density, between 0.005 and 2 V vs Na/Na$^+$. At the first cycle, charge/discharge capacities of HS-HTC@500, HS-HTC@750, and HS-HTC@1000 are 83/384 mAh $\times$ g^{-1} with an initial coulombic efficiency of 21.6%, 137/300 mAh $\times$ g^{-1} with an initial coulombic efficiency of 45.6% and 232/472 mAh $\times$ g^{-1} with an initial coulombic efficiency 49.1%, respectively. At the end of 100 cycles, HS-HTC@500 electrode delivered specific capacity of 54 mAh $\times$ g^{-1} with a capacity retention of 14%. HS-HTC@750 electrode delivered specific capacity of 122 mAh $\times$ g^{-1} with a capacity retention of 40.6% and HS-HTC@1000 electrode delivered specific capacity of 196 mAh $\times$ g^{-1} with a capacity retention of 41.5%.

The high irreversible capacity and low initial coulombic efficiency (ICE) are the results of the irreversibly intercalated sodium ions to the surface defects of hard carbon and the reaction between sodium ions and functional groups present on the surface. Solid electrolyte interphase (SEI) formation as a result of the decomposition of electrolyte can also cause the low ICE [36]. Thus, the sample treated at 1000 °C, HS-HTC@1000, has superior electrochemical performance that can be explained by its higher electrical conductivity.

Later, in order to study the binder effect on electrode performances, three different binders were tested with HS-HTC@1000 electrode shown in Figure 5. PVdF is the most widely used binder due to its good electrochemical performance. However, it was reported that the defluorination of PVdF can cause damage on hard carbon electrode [37]. As alternative binders, CMC, Na-alginate, and PAA can be suggested by their water-soluble character making them environmentally friendly in nature.
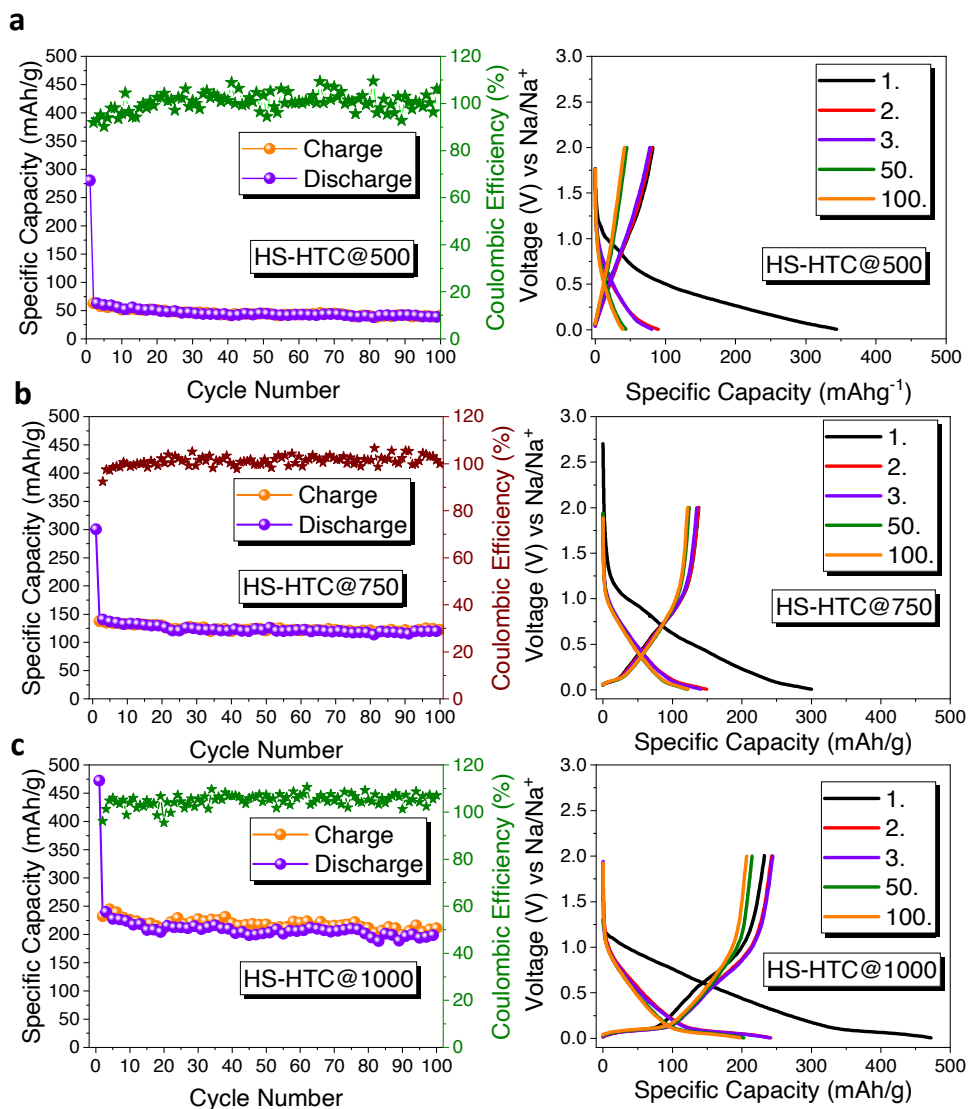
Figure 4. Cycle performances and galvanostatic charge/discharge curves of a) HS-HTC@500, b) HS-HTC@750, c) HS-HTC@1000 (Note: Electrodes were tested with PVdF binder).

Initially, CMC binder was tested delivering the first charge/discharge capacities as 92/172 mAh × g^{-1} with an initial coulombic efficiency of 53.4% (Figure 5a). After 100 cycles, the electrode has 219 mAh × g^{-1} specific capacity. Then, Na-alginate binder was performed, and the electrode delivered around 230/404 mAh × g^{-1} charge/discharge capacities with a 55.6 % initial coulombic efficiency (Figure 5b). At the end of 100 cycles, the electrode demonstrated 232 mAh × g^{-1} specific capacity with a capacity retention of 57.4%. Lastly, PAA binder was performed, shown in Figure 5c, and the electrode delivered around 199/361 mAh × g^{-1} charge/discharge capacities with a 55.1% initial coulombic efficiency. Then the electrode yielded around 183 mAh × g^{-1} specific capacity with a capacity retention of 50.6% after 100 cycles. As a whole, when the binders' impacts were compared, Na-alginate binder yielded a superior performance than that of the others. Na-alginate is a natural polysaccharide that contains carboxylic groups on each monomer units. CMC binder is cellulose derivative and produced synthetically, also has carboxylic groups on monomer units, but they are distributed randomly. These chemical differences between the two binders can explain the better electrode performance with Na-alginate binder. Uniform carboxylic groups can ensure stable SEI layer and homogeneous coverage [38]. Here, the resulting HS-based hard carbon electrodes were compared in terms of their electrochemical performances in Table 1. The effect of both hydrothermal carbonization and further carbonization temperature can be seen from the table. Among all samples that are investigated in this study, the composites synthesized at 1000 °C show the best results.
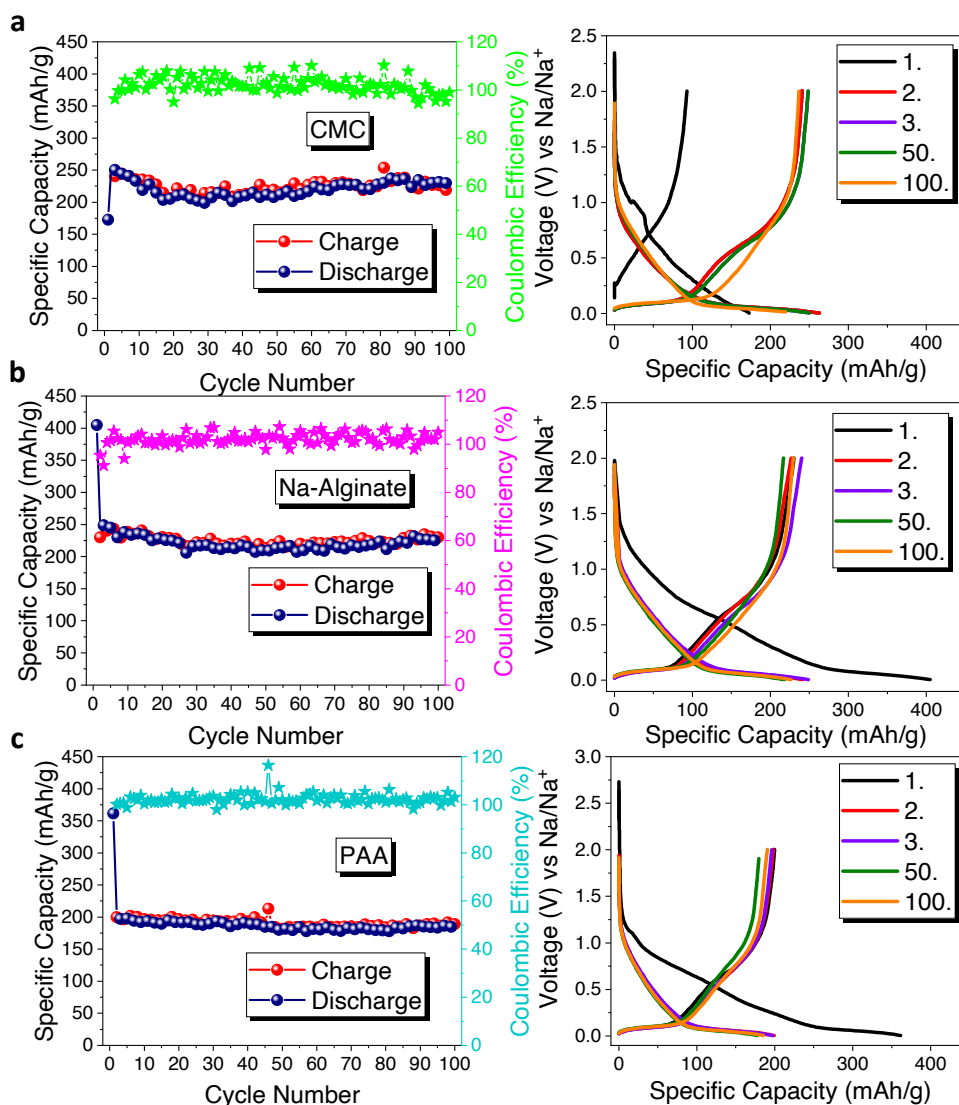
Figure 5. Cycle performances and galvanostatic charge/discharge curves of HS-HTC@1000 electrode with a) CMC, b) Na-alginate, and c) PAA binders.

Lastly, biomass-derived hard carbon electrodes reported in the literature as anodes for sodium ion batteries are shown in Table 2. Most of the hard carbons are produced from widely available agricultural waste, with a focus on elucidating the effect of carbonization processes and impact of binders. Thus, based on the comparison given in Table 2, it is clearly seen that HS-derived hard carbon can be promising anode materials for sodium ion batteries. To sum up, Figure 6 represents the comparison of the HS-HTC@1000 electrode with different binders emphasizing the best performance of the Na-alginate binder.

The impact of binders was further evaluated by impedance measurements. Figure 7 shows the Nyquist plots of HS-HTC@1000 electrode with CMC, Na-alginate and PVdF binders and the equivalent electric circuits were demonstrated as inset images. Impedance fitting parameters can be listed as the electrolyte resistance (R1): the charge transfer resistance (R2∥Q2): the solid electrolyte interface resistance (R3∥Q3): the restricted diffusion element (M) [39] and the results are shown in Table 3. All electrodes have one depressed semicircle in the high frequency and a straight line in low frequency. The semicircle at higher frequency is referred to the SEI formation on the surface and the charge transfer resistance at interface. Obviously, there is a difference between initial and after cycling resistances. PVdF showed the smaller semicircle diameter when compared with the other binders at the initial condition. From the observation of Figure 7 for PVdF binder, an increase of depressed-semicircle diameter was determined. Na-alginate and CMC binders have more stable SEI film

Table 1. Cycle performances of electrodes.

| Electrode	Binder	Cycle number	Capacity (mAh × g^{-1}) discharge-charge
HS@500	PVdF	1	280–63
		100	41–39
HS@750	PVdF	1	321–121
		100	48–61
HS@1000	PVdF	1	283–93
		100	101–100
HS-HTC@500	PVdF	1	344–83
		100	54–53
HS-HTC@750	PVdF	1	300–137
		100	122–122
HS-HTC@1000	PVdF	1	472–232
		100	196–210
HS-HTC@1000	CMC	1	172–92
		100	219–236
HS-HTC@1000	Na-alginate	1	404–230
		100	232–231
HS-HTC@1000	PAA	1	361–199
		100	183–190

Table 2. Biomass-derived hard carbon anodes for sodium ion batteries.

Biomass precursor	Reversible capacity	Current density	Ref.
Lotus stem	250 mAh × g^{-1}	100 mA × g^{-1}	[44]
Rice husk	276 mAh × g^{-1}	0.1 C	[45]
Grass	200 mAh × g^{-1}	100 mA × g^{-1}	[46]
Mangosteen shell	330 mAh × g^{-1}	20 mA × g^{-1}	[47]
Apricot shell	184 mAh × g^{-1}	0.1 C	[21]
Rambutan peel	225 mAh × g^{-1}	0.1 C	[22]
Tea leaves	179 mAh × g^{-1}	100 mA × g^{-1}	[48]
Macadamia nutshell	220 mAh × g^{-1}	20 mA × g^{-1}	[49]
Unburned charcoal	292.3 mAh × g^{-1}	50 mA × g^{-1}	[50]
Hazelnut shell	232 mAh × g^{-1}	0.1 C	this study

formation. Moreover, defluorination of PVdF binder can be considered to additional interface and the side reactions can increase the resistance [6]. On the other hand, for CMC (R$_{initial}$: 1829.7 ohm, R$_{total}$: 318.4 ohm) and Na-alginate (R$_{initial}$: 1671.8 ohm, R$_{total}$: 514.3 ohm) binders, the initial resistance values were much higher than those after cycling. This was opposite for the PVdF binder, in which the initial total resistance was much lower than that of after cycling (R$_{initial}$: 1621.7, ohm R$_{total}$: 3058.4 ohm) supporting the defluorination of PVdF. Na-alginate and CMC binders have strong adhesion performance and uniform distribution on the electrode surface which ensure lower charge resistance. Smaller total resistance demonstrates that Na-alginate and CMC binders have more stable SEI layer [38, 40, 41]. Lower charge transfer resistance can ensure better cycling performance and kinetic properties of electrode [36].
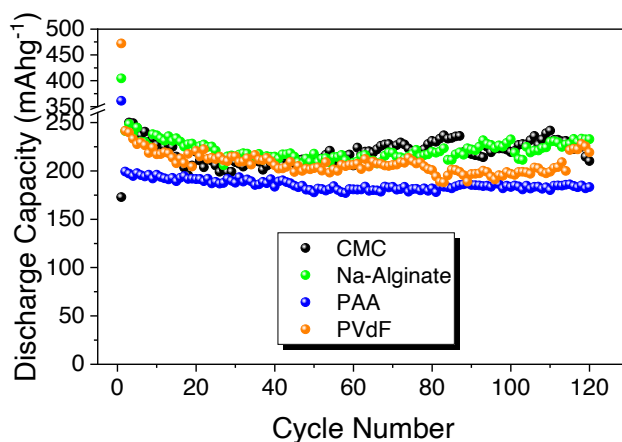
Figure 6. Discharge capacity comparison of HS-derived hard carbon electrode (HS-HTC@1000) with PVdF, CMC, Na-alginate, PAA binders.
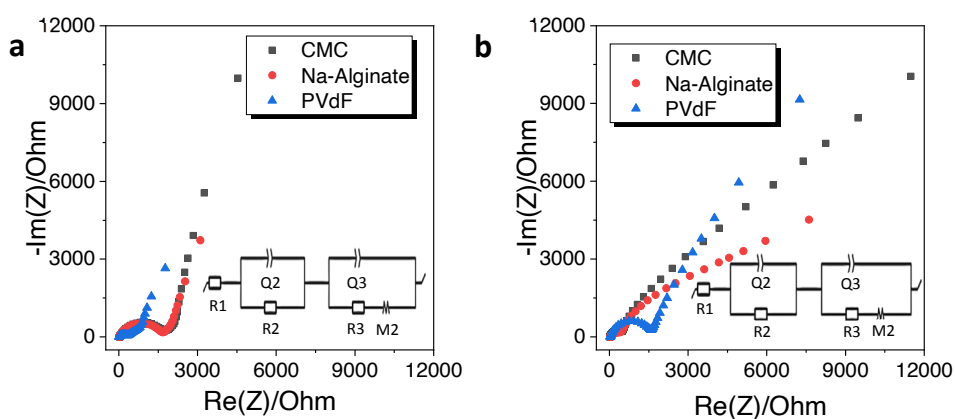
Figure 7. Electrochemical impedance spectra of HS-HTC@1000 with CMC, Na-alginate, and PVdF binders a) initial, b) after 10 charge/discharge cycles.

Table 3. Impedance fitting parameters.

	CMC	Na-alginate	PVdF
Before cycles			
R_1 (Ω)	33.24	9.523	5.579
R_2 (Ω)	1660	1660	322.2
R_3 (Ω)	136.5	2.289	1294
After cycles			
R_1 (Ω)	17.97	37.39	35.47
R_2 (Ω)	297	476.8	1590
R_3 (Ω)	3.455	0.11	1433

CV analysis at different scan rates were also performed for the HS-HTC@1000 electrode at 0.2, 0.1, 0.05, 0.01 mV × s^{-1} (Figure 8a). Equation (1) was used to be able to calculate the capacitive and diffusion-controlled contributions.

$$i(V) = k_1 v + k_2 v^{1/2} \tag{1}$$

At a fixed potential, $k_1 v$ represents capacitive current, $k_2 v^{1/2}$ indicates diffusion controlled current. When equation (1) is rearranged (scan rate: v, constant: k_1 and k_2) and plotted versus $i/v^{1/2}$ to $v^{1/2}$, k_1 refers to slope and k_2 is the intercept (Figure
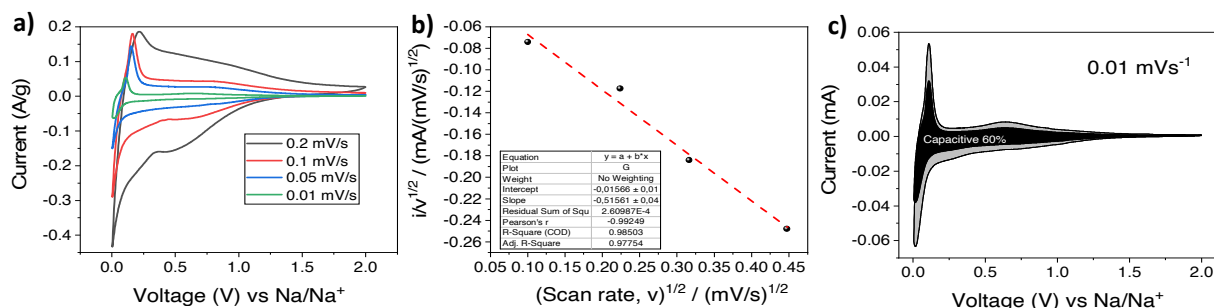
Figure 8. a) CV curves at various scan rates (0.2, 0.1, 0.05, 0.01 mV × s⁻¹.) b) i/v $^{1/2}$ vs v $^{1/2}$ plot, c) capacitive contribution (black) and diffusion contribution (grey) at 0.01 mV × s⁻¹.

8b) [42,43]. Then, the contribution ratios were analyzed for all sweep rates by peaking up the voltage values from 0.2 to 1.0 V (vs Na) at every 0.1 interval. Figure 8c demonstrates the results from the scan rate of 0.01 mV × s⁻¹ in which the capacitive contribution of the total capacity is 60%. As expected, the proportion of capacitive contribution increased with the scan rate (60%, 77%, 82% where the scan rates are 0.01, 0.05, 0.1 mV × s⁻¹, respectively).

4. Conclusions

In summary, we have effectively synthesized hazelnut shell-derived low-cost hard carbons by using hydrothermal treatment and further carbonization at different temperatures. After further carbonization process, all the samples have layer distances larger than the graphite which is suitable for sodium ion storage. Hard carbon prepared at 1000 °C with sodium alginate binder yielded superior electrochemical performance as anode for sodium ion battery with a reversible capacity of 232 mAh × g⁻¹ at 0.1 C current density. This promising performance along with the simple, economical, and scalable synthesis process can make biomass-derived hard carbon a promising anode material for sodium ion batteries. Besides, water-soluble binders show that environmentally friendly binders can be potential candidates for conventional PVdF binder.

References

1. Tarascon JM, Armand M. Issues and challenges facing rechargeable lithium batteries. Nature 2001; 414 (6861): 359-67. doi: 10.1038/35104644

2. Goodenough JB, Kim Y. Challenges for Rechargeable Li Batteries. Chemistry of Materials 2010; 22 (3): 587-603. doi: 10.1021/cm901452z

3. Dunn B, Kamath H, Tarascon JM. Electrical energy storage for the grid: a battery of choices. Science 2011; 334 (6058): 928-935. doi: 10.1126/science.1212741

4. Ellis BL, Nazar LF. Sodium and sodium-ion energy storage batteries. Current Opinion in Solid State and Materials Science 2012; 16 (4): 168-177. doi: 10.1016/j.cossms.2012.04.002

5. Nayak PK, Yang L, Brehm W, Adelhelm P. From lithium-ion to sodium-ion batteries: advantages, challenges, and surprises. Angewandte Chemie International Edition 2018; 57 (1): 102-120. doi: 10.1002/anie.201703772

6. Dahbi M, Yabuuchi N, Kubota K, Tokiwa K, Komaba S. Negative electrodes for Na-ion batteries. Physical Chemistry Chemical Physics 2014; 16 (29): 15007-15028. doi: 10.1039/c4cp00826j

7. Jache B, Adelhelm P. Use of graphite as a highly reversible electrode with superior cycle life for sodium-ion batteries by making use of cointercalation phenomena. Angewandte Chemie International Edition 2014; 53 (38): 10169-10173. doi: 10.1002/anie.201403734

8. Ponrouch A, Palacin MR. On the high and low temperature performances of Na-ion battery materials: Hard carbon as a case study. Electrochemistry Communications 2015; 54 51-54. doi: 10.1016/j.elecom.2015.03.002

9. Hou H, Qiu X, Wei W, Zhang Y, Ji X. Carbon anode materials for advanced sodium-ion batteries. Advanced Energy Materials 2017; 7 (24): 1602898. doi: 10.1002/aenm. 201602898

10. Wen Y, He K, Zhu Y. Expanded graphite as superior anode for sodium-ion batteries. Nature Communications 2014; 5: 4033. doi: 10.1038/ncomms5033

11. Li Y, Hu YS, Li H, Chen L, Huang X. A superior low-cost amorphous carbon anode made from pitch and lignin for sodium-ion batteries. Journal of Materials Chemistry A 2016, 4: 96-104. doi: 10.1039/c5ta08601a

12. Zhou H, Li X, Li Y, Zheng M, Pang H. Applications of M x Se y (M ¼ Fe, Co, Ni) and their composites in electrochemical energy storage and conversion. Nano-Micro Letters 2019; 11 (1). doi: 10.1007/s40820-019-0272-2

13. Zhang N, Han X, Liu Y, Hu X, Zhao Q et al. 3D Porous γ-Fe 2 O 3 @C nanocomposite as high-performance anode material of Na-ion batteries. Advanced Energy Materials 2015, 5: 1401123. doi: 10.1002/aenm.201401123

14. Lao M, Zhang Y, Luo W, Yan Q, Sun W et al. Alloy-based anode materials toward advanced sodium-ion batteries. Advanced Materials 2017; 29 (48): 1700622–1700623. doi: 10.1002/adma.201700622

15. Fang Y, Xu X, Du Y, Zhu X, Zhou X et al. Novel nitrogen-doped reduced graphene oxide-bonded Sb nanoparticles for improved sodium storage performance. Journal of Materials Chemistry A 2018; 6: 11244. doi: 10.1039/c8ta02945h

16. He M, Kravchyk K, Walter M, Kovalenko M. Monodisperse antimony nanocrystals for high-rate Li-ion and Na-ion battery anodes: nano versus B. NanoLetters 2014; 14: 1255-1262. doi: 10.1021/nl404165c

17. Wang H, Zhang X. Organic carbonyl compounds for sodium-ion batteries: recent progress and future perspectives. Chemistry 2018; 24: 18235–18245. doi: 10.1002/chem. 201802517

18. Zhao L, Zhao J, Hu YS, Li H, Zhou Z et al. Disodium Terephthalate (Na$_2$C$_8$H$_4$O$_4$) as high performance anode material for low-cost room-temperature sodium-ion battery. Advanced Energy Materials 2012; 2: 962-965. doi: 10.1002/aenm.201200166

19. Luo C, Shea JJ, Huang J. A carboxylate group-based organic anode for sustainable and stable sodium ion batteries. Journal of Power Sources 2020; 453: 227904. doi: 10.1016/j.jpowsour.2020.227904

20. Chevrier VL, Ceder G. Challenges for Na-ion negative electrodes. Journal of the Electrochemical Society 2011; 158 (9): A1011-A1014. doi: 10.1149/1.3607983

21. Demir E, Aydin M, Arie AA, Demir-Cakan R. Apricot shell derived hard carbons and their tin oxide composites as anode materials for sodium-ion batteries. Journal of Alloys and Compounds 2019; 788: 1093-1102. doi: 10.1016/j.jallcom.2019.02.264

22. Arie AA, Kristianto H, Muljana H, Stievano L. Rambutan peel based hard carbons as anode materials for sodium ion battery. Fullerenes, Nanotubes and Carbon Nanostructures 2019; 27 (12): 953-960. doi: 10.1080/1536383X.2019.1671372

23. Guney MS. Utilization of hazelnut husk as biomass. Sustainable Energy Technologies and Assessments 2013; 4: 72-77. doi: 10.1016/j.seta.2013.09.004

24. Pérez-Armada L, Rivas S, González B, Moure A. Extraction of phenolic compounds from hazelnut shells by green processes. Journal of Food Engineering 2019; 255: 1-8. doi: 10.1016/j.jfoodeng.2019.03.008

25. Liu T, Li XF. Biomass-derived nanostructured porous carbons for sodium ion batteries: a review. Materials Technology 2019; 34 (4): 232-245. doi: 10.1080/10667857.2018.1545392

26. Demirbas A. Properties of charcoal derived from hazelnut shell and the production of briquettes using pyrolytic oil. Energy 1999; 24 (2): 141-150. doi: 10.1016/S0360-5442(98)00077-2

27. Zhang S, Li Y, Li M. Porous hard carbon derived from walnut shell as an anode material for sodium-ion batteries. The Journal of The Minerals, Metals & Materials Society 2018; 70: 1387–1391. doi: 10.1007/s11837-018-2789-0

28. Manić NG, Janković BŽ, Stojiljković DD, Jovanović VV, Radojević MB. TGA-DSC-MS analysis of pyrolysis process of various agricultural residues. Thermal Science 2019; 23: 1457-1472. doi: 10.2298/TSCI180118182M

29. Xie F, Xu Z, Guo Z, Titirici MM. Hard carbons for sodium-ion batteries and beyond. Progress in Energy 2020; 2: 042002. doi: 10.1088/2516-1083

30. Alptekin H, Au H, Jensen CS A, Olsson E, Goktas M et al. Sodium storage mechanism investigations through structural changes in hard carbons. ACS Applied Energy Materials 2020; 3 (10): 9918-9927. doi: 10.1021/acsaem.0c01614

31. Kumar M, Gupta RC, Sharma T. X-ray diffraction studies of Acacia and Eucalyptus wood chars. Journal of Materials Science 1993; 28 (3): 805-810.

32. Zhang N, Liu Q, Chen W, Wan M, Li X et al. High capacity hard carbon derived from lotus stem as anode for sodium ion batteries. Journal of Power Sources 2018; 378: 331-337. doi:10.1016/j.jpowsour.2017.12.054

33. Sevilla M, Fuertes AB. Chemical and structural properties of carbonaceous products obtained by hydrothermal carbonization of saccharides. Chemistry – A European Journal 2009; 15 (16): 4195-4203. doi: 10.1002/chem.200802097

34. Wang L, Schnepp Z, Titirici MM. Rice husk-derived carbon anodes for lithium ion batteries. Journal of Materials Chemistry A 2013; 1 (17). doi: 10.1039/C3TA10650K

35. Falco C, Baccile N, Titirici MM. Morphological and structural differences between glucose, cellulose and lignocellulosic biomass derived hydrothermal carbons. Green Chemistry 2011; 13 (11): 3273-3281. doi: 10.1039/C1GC15742F

36. Aydin M, Demir E, Unal B, Dursun, B, Ahsen AS et al. Chitosan derived N-doped carbon coated SnO2 nanocomposite anodes for Na-ion batteries. Solid State Ionics 2019; 341. doi: 10.1016/j.ssi.2019.115035

37. Zhang WJ, Dahbi M, Komaba S. Polymer binder: a key component in negative electrodes for high-energy Na-ion batteries. Current Opinion in Chemical Engineering 2016; 13: 36- 44. doi: 10.1016/j.coche.2016.08.001

38. Kovalenko I, Zdyrko B, Magasinski A, Hertzberg B, Milicev Z et al. A major constituent of brown algae for use in high-capacity Li-Ion batteries. Science 2011; 334 (6052): 75-79. doi: 10.1126/science.1209150

39. Bayram O, Kiskan B, Demir E, Remir Cakan R, Yagci Y. Advanced thermosets from sulfur and renewable benzoxazine and ıonones via ınverse vulcanization. ACS Sustainable Chemistry & Engineering 2020 8 (24): 9145-9155 doi: 10.1021/acssuschemeng.0c02773

40. Arie AA, Kristianto H, Demir E, Demir Cakan R. Activated porous carbons derived from the Indonesian snake fruit peel as anode materials for sodium ion batteries. Material Chemistry and Physics 2018 (217): 254-261. doi: 10.1016/j.matchemphys

41. Dogrusoz M, Demir Cakan R. Mechanochemical synthesis of SnS anodes for sodium ion batteries. International Journal of Energy Research 2020; 44: 10809-10820.

42. Wang J, Polleux J, Lim J, Dunn B. Pseudocapacitive contributions to electrochemical energy storage in TiO2 (Anatase) nanoparticles. Journal of Physical Chemistry C 2007; 111 (40): 14925–14931. doi: 10.1021/jp074464w

43. Halim EM, Demir-Cakan R, Debiemme-Chouvy C, Perrot H et al. Poly (ortho -phenylenediamine) overlaid fibrous carbon networks exhibiting synergistic effect for enhanced performance in hybrid micro energy storage devices. Journal of Materials Chemistry A. 2021 9(16). doi: 10.1039/D1TA00763G.

44. Zhang N, Liu Q, Chen W, Wan M, Li X et al. High capacity hard carbon derived from lotus stem as anode for sodium ion batteries. Journal of Power Sources 2018; 378: 331-337. doi: 10.1016/j.jpowsour.2017.12.054

45. Rybarczyk MK, Li Y, Qiao M, Hu YS, Titirici MM et al. Hard carbon derived from rice husk as low cost negative electrodes in Na-ion batteries, Journal of Energy Chemistry 2019; 29: 17-22. doi: 10.1016/j.jechem.2018.01.025

46. Zhang F, Yao Y, Wan J, Henderson D, Zhang X et al. High Temperature Carbonized Grass as a High Performance Sodium Ion Battery Anode. ACS Applied Materials & Interfaces 2017; 9 (1): 391-397 doi: 10.1021/acsami.6b12542

47. Wang K, Jin Y, Sun S, Huang Y, Peng J. Low-cost and high-performance hard carbon anode materials for sodium-ion batteries. ACS Omega 2017; 2: 1687-1695. doi: 10.1021/acsomega.7b00259.

48. Arie, AA, Tekin, B, Demir E, Demir-Cakan R. Utilization of the Indonesian's spent tea leaves as promising porous hard carbon precursors for anode materials in sodium ion batteries. Waste Biomass Valorization 2020; 11: 3121–3131. doi: 10.1007/s12649-019-00624-x

49. Kumar U, Wu J, Sharma N, Sahajwalla V. Biomass derived high areal and specific capacity hard carbon anodes for sodium-ion batteries. Energy & Fuels 2021; 35 (2): 1820-1830 doi: 10.1021/acs.energyfuels.0c03741

50. Yu HY, Liang HJ, Gu ZY, Meng YF, Yang M et al. Waste-to-wealth: low-cost hard carbon anode derived from unburned charcoal with high capacity and long cycle life for sodium-ion/lithium-ion batteries. Electrochimica Acta 2020; 361: 137041, ISSN 0013-4686. doi: 10.1016/j.electacta.2020.137041